UC Riverside
2018 Publications

Title
Outlier accommodation for meter-level positioning: Risk-averse performance-specified state estimation

Permalink
https://escholarship.org/uc/item/4d39730v

Authors
Aghapour, E.
Rahman, F.
Farrell, J.A.

Publication Date
2018

Peer reviewed

eScholarship.org Powered by the California Digital Library
University of California

Outlier Accommodation for Meter-level Positioning: Risk-Averse Performance-Specified State Estimation

Elahe Aghapour, Farzana Rahman and Jay A. Farrell
Department of Electrical and Computer Engineering, University of California, Riverside, 92521.
{eaghapour, frimi, farrell}@ee.ucr.edu

***Abstract*—Autonomous vehicle operation would be enhanced if a specified level of accuracy could be guaranteed. Risk-averse performance-specified (RAPS) state estimation works within an optimization setting to choose the set of measurements that achieves a performance specification with minimum risk of inclusion of outliers. This paper considers the challenge of preventing outlier measurements from affecting the accuracy and reliability of state estimation, with minimal risk. This paper is that for the first time applies the RAPS approach to the GNSS vehicle state estimation problem, including a review of the theoretical derivation and experimental results. The experimental results utilize real-world Doppler and differential pseudorange data that allows a comparative study with the standard Neyman-Pearson (NP) approach and RAPS state estimation.**

I. INTRODUCTION

Autonomous and connected vehicle applications would be enhanced by reliable full-state estimation consistent with submeter positioning accuracy. While GNSS-based navigation has increased drastically in recent decades, even for differential applications reliable submeter positioning accuracy is challenging due to the presence of outliers in GNSS measurements that may be caused for example by multipath, overhead foliage, or non-line-of-sight signals (see Chapter 26 in [1]). This is especially true in urban environments.

In general, land vehicle navigation applications are signal rich: images contain many features, IMU's are viable, and GNSS comprises many separate systems (e.g., GPS, GLONASS, BeiDou, Galileo) each of which over-supplies the number of satellites necessary for state estimation. To achieve a specified level of state estimation accuracy, the full set of measurements is typically not required, so long as the measurements that are used are valid (i.e., outlier free). Therefore, if the full set of measurements was used, then the state estimate would have been exposed to unnecessary risk, while the computed covariance would show that the estimator is over-performing relative to the specification. In reality, outliers are likely to have been included, making the state estimate incorrect and the covariance overly confident in that incorrect estimate. Therefore, outlier accommodation is both possible (due to redundancy) and important.

The literature discusses various outlier detection techniques building on fundamental ideas [2]–[7]. The RAIM techniques are based on computing a party vector from the measurement residual [8]–[11] assuming that there is enough measurement redundancy to discriminate the outlier source. While many RAIM approaches assume that there is only one outlier, multiple outlier detection has also been well developed [9], [10], [12]–[14]. Extended RAIM (eRAIM) [15] incorporates an Inertial Measurement Unit (IMU) and Kalman filter based estimation into RAIM.

Data redundancy, quantified by the number of degrees-of-freedom (DOFs), is critical to successful outlier accommodation. Both RAIM and eRAIM are based on measurements from a single epoch, limiting data redundancy. Redundancy can be enhanced both by adding additional sensors or by solving the estimation problem using all sensor data within a sliding temporal window.

The outlier detection problem is fundamentally unobservable, when all measurements have the potential to be affected by outliers [16], [17]. Therefore, outlier detection methods such as those reviewed above are built on outlier hypothesis assumptions, resulting in tests to choose the most likely assumption. When the number of possible hypothesis assumptions is too low, the actual outlier scenario may not be included, but the required level of computations increases with the number and complexity of the assumed fault scenarios.

Recently new methods for outlier accommodation without explicit detection have been presented in the literature. The Least Soft-thresholded Squares (LSS) approach, building on l_1-regularization, that was presented in [18]–[22]. A version of the LSS approach adapted to the problem of [23] is presented in [24]. Alternatively, [16] works within an optimization setting to find the largest set of measurements self-consistent with the assumed model. Finally, [17] works within an optimization setting to choose the set of measurements that achieves a performance specification with minimum risk. The performance specification is phrased in terms of the posterior information matrix. The method is able to quantify when the performance specification is feasible and to quantify the risk associated with the achieved level of performance. The risk is defined by the norm of the covariance normalized residual vector. Reference [17] works in a general theoretical setting, with generic academic examples and no in-depth evaluation has been conducted so far.

The main contribution of this paper is that for the first time, the risk-averse performance-specified approach of [17] will be applied to and explained for the GNSS state estimation problem, including both the theoretical derivation and experimental results. The experimental results utilize real-world Doppler and differential pseudorange data, considering the risk associated with both sets of measurements.

978-1-5386-1647-5/18/$31.00 ©2018 IEEE

The next section presents the problem statement for the GNSS/IMU state estimation problem. Section III quickly reviews the risk-averse performance-specified state estimation method. Presentation and evaluation of experimental results follows in Section IV.

II. PROBLEM STATEMENT

This section introduces GNSS navigation system background and notation [25].

The rover state estimation algorithm has two steps: time propagation and measurement update. This article considers the standard position, velocity, acceleration (PVA) model for the time propagation step. GNSS pseudorange and Doppler used for the measurement update. This section introduces the PVA and GNSS models.

A. Time Propagation

Let $x = [p^\top, v^\top, a^\top, t_r, b_r, M_r]^\top \in \mathbb{R}^{n_s}$ denote the rover state vector, where p, v and $a \in \mathbb{R}^3$ represent the rover position, velocity, and acceleration vectors, respectively. The symbols $t_r, b_r \in \mathbb{R}^1$ represent the receiver clock bias and drift rate. The symbol $M_r \in \mathbb{R}^m$ represent the multipath state, where m is the number of GNSS measurements available. Thus, the dimension of the state vector is $n_s = 11 + m$.

The rover state propagates forward through time as

$$x_{i+1} = \Phi_T x_i + \omega_i. \tag{1}$$

The matrix

$$\Phi_T = \begin{bmatrix} \boldsymbol{I}_3 & T\boldsymbol{I}_3 & T^2\boldsymbol{I}_3 & \mathbf{0} & \mathbf{0} & \mathbf{0} \\ \mathbf{0} & \boldsymbol{I}_3 & T\boldsymbol{I}_3 & \mathbf{0} & \mathbf{0} & \mathbf{0} \\ \mathbf{0} & \mathbf{0} & \boldsymbol{I}_3 & \mathbf{0} & \mathbf{0} & \mathbf{0} \\ \mathbf{0} & \mathbf{0} & \mathbf{0} & 1 & T & \mathbf{0} \\ \mathbf{0} & \mathbf{0} & \mathbf{0} & 0 & 1 & \mathbf{0} \\ \mathbf{0} & \mathbf{0} & \mathbf{0} & \mathbf{0} & \mathbf{0} & \boldsymbol{I}_m \end{bmatrix} \tag{2}$$

where $\boldsymbol{I}_q$ is the identity matrix for $\mathbb{R}^q$ and the symbol $\mathbf{0}$ a zero matrix with the number of rows and columns necessary to conform. The propagation matrix Φ_T is constant over time. The length of the time propagation step is T. Using the symbols η_a, η_d and η_m to represent the acceleration, clock drift and multipath state process noise, respectively, then $\omega_i \sim \mathcal{N}(0, Q_d)$ represents the integrated effect of process noise vector $\omega = [0\ 0\ \eta_a^\top\ 0\ \eta_d\ \eta_m^\top]^\top$ over time interval T.

Let t_{k-1} and t_k represent the time of the previous and current GNSS measurements. Let $N_p = \frac{(t_k - t_{k-1})}{T}$) be a whole number. The rover state integrates the expected value of eqn. 1. Therefore,

$$\hat{x}_k^- = (\Phi_T)^{N_p}\, x_{k-1}^+ \tag{3}$$

The covariance of the state error over the interval $[t_{k-1}, t_k]$ accumulates as

$$P_k^- = \Phi P_{k-1}^+ \Phi^\top + Q_d \tag{4}$$

where P_k^- is the prior covariance and $\Phi = (\Phi_T)^{N_p}$.

B. Measurements

Our experiment uses single-differenced GNSS pseudorange measurement [25] that will be denoted as $\Delta\tilde{\rho}_r^s(k)$. The single-differenced GNSS pseudorange measurement model is

$$\Delta\rho_r^s(k) = R(p_k, \hat{p}_k^s) + c\,t_r(k) + M_r^s(k) + \eta_r^s(k) \tag{5}$$

where $R(p_k, p_k^s) = \|p_k - \hat{p}_k^s\|$ is the range from receiver r to satellite s, $c\,t_r$ is receiver clock bias in meters, M_r^s is multipath error for satellite s, and $\eta_r^s \sim \mathcal{N}(0, R_p)$ is random pseudorange measurement noise.

Linearization of the single-differenced pseudorange measurement at $\hat{p}_k^-$ yields the measurement model

$$\Delta\rho_r^s(k) = R(\hat{p}_k^-, \hat{p}_k^s) + h_k(p_k - \hat{p}_k^-) + ct_{rk} + M_r^s(k) + \eta_{rk}^s$$

where $h_k^s = \frac{p_k^- - \hat{p}_k^s}{\|p_k^- - \hat{p}_k^s\|}$ is the line-of-sight vector from receiver r to satellite s. The psuedorange measurement residual is computed as

$$\delta\rho_r^s(k) = \Delta\tilde{\rho}_r^s(k) - R(\hat{p}_k^-, \hat{p}_k^s) - \hat{M}_r^s(k)$$

and modeled as

$$\delta\rho_r^s(k) = h_k^s \delta p_k + ct_{rk} + \delta M_r^s(k) + \eta_r^s(k)$$

where $\delta p_k = p_k - \hat{p}_k^-$ and $\delta M_r^s(k) = M_r^s(k) - \hat{M}_r^s(k)$.

After correction for the satellite velocity, the Doppler measurement model is:

$$\lambda D_r^s(k) = h_k^s v_k + cb_r(k) + \varepsilon_r^s(k) \tag{6}$$

where v is the rover velocity vector, ε_r^s is measurement noise with $\varepsilon_r^s(k) \sim \mathcal{N}(0, R_d)$. The Doppler measurement is linear in the rover velocity. The Doppler residual is computed as

$$\delta D_r^s(k) = \lambda\tilde{D}_r^s(k) - \left(h_k^s \hat{v}_k + c\hat{b}_r(k)\right)$$

and modeled as

$$\delta D_r^s(k) = h_k^s \delta v_k + c\delta b_r(k) + \varepsilon_r^s(k)$$

where $\delta v_k = v_k - \hat{v}_k^-$ and $\delta b_r(k) = b_r(k) - \hat{b}_r(k)$.

The measurement vector for satellite s is

$$z_k^s = \begin{bmatrix} \delta\rho_r^s(k) \\ \delta D_r^s(k) \end{bmatrix}. \tag{7}$$

The linearized measurement model has the form

$$z_k^s = H_k^s \delta x_k + \gamma_r^s(k) \tag{8}$$

where $\delta x_k = x_k^- - \hat{x}_k^-$. The measurement matrix is

$$H_k^s = \begin{bmatrix} h_k^s & 0 & 0 & 0 & 0 & 1 & 0 & \cdots & 1 & \cdots \\ 0 & h_k^s & 0 & 0 & 0 & 0 & 1 & \cdots & 0 & \cdots \end{bmatrix} \tag{9}$$

where the rightmost 1 in the first row corresponds to element s of the multipath vector. The noise vector

$$\gamma_{rk}^s = \begin{bmatrix} \eta_{rk}^s \\ \varepsilon_{rk}^s \end{bmatrix} \sim \mathcal{N}(0, R) \text{ where } R = \begin{bmatrix} R_p & 0 \\ 0 & R_d \end{bmatrix}.$$

C. Notation

The presentation will use information vectors and matrices. For a random variable with distribution $\mathcal{N}(\mu, P)$ a canonical representation of is given by the information matrix $J = P^{-1}$ and the information vector $\zeta = P^{-1}\mu$.

Corresponding to the optimal gain, the measurement update for the covariance is

$$P_k^+ = (I - K_k H_k) P_k^- . \tag{10}$$

Corresponding to eqns. (4) and (10), the time and (optimal) measurement update equations for the information matrix are [26]:

$$\begin{aligned} J_k^- &= (\Phi(J_{k-1}^+)^{-1}\Phi^\top + Q_d)^{-1} \\ J_k^+ &= H_k^\top R^{-1} H_k + J_k^- . \end{aligned} \tag{11}$$

The assumption of Gaussian noise will naturally result in squared Mahalanobis norms for the optimizaion problems. The squared Mahalanobis norm of vector r with covariance C is denoted by $||r||_C^2 = r^\top C^{-1} r = ||\Sigma r||_2^2$ where $C^{-1} = \Sigma^\top \Sigma$.

III. PROBLEM SOLUTION

A main new idea of [16], [17] was to change the focus from detecting outliers to find a subset of the measurements that can be consistently produced by the assumed measurement model and satisfying the accuracy specification.

In the standard Maximum A Posteriori (MAP) state estimation approach, using all measurements at time k, the negative log-likelihood of the distribution yields the optimization

$$\begin{aligned} x_k^\star = \underset{x_k}{\operatorname{argmin}} \big(& \|\Phi x_{k-1} - x_k\|_{Q_d}^2 \\ & + \|x_{k-1} - \hat{x}_{k-1}^+\|_{P_{k-1}^+} + \|H_k x_k - z_k\|_R^2 \big) \end{aligned} \tag{12}$$

where $\hat{x}_{k-1}^+$ represents the optimal a posteriori estimate at time $k-1$.

In this paper, the prior and state transition are always trusted (i.e., outlier-free). Therefore, the first and second term of the optimization can be propagated to produce $\hat{x}_k^-$ and P_k^- using eqns. (3) and (4). This simplifies eqn. (12) to the equivalent problem

$$x_k^\star = \underset{x_k}{\operatorname{argmin}} \big(\|x_k - \hat{x}_k^-\|_{P_k^-} + \|H_k x_k - z_k\|_R^2 \big) \tag{13}$$

The solution to eqn. (13) is the standard (extended) Kalman filter for the GPS INS problem.

To find the optimal measurement subset, a binary selection vector $b = (b_1 \quad b_2 \quad \cdots \quad b_m)^\top$ is introduced. The selection variable b_i, associated with i^{th} measurement, is used to disable or enable a measurement with $b_i = 0$ and $b_i = 1$, respectively. The optimization works on an augmented problem, searching for a state estimate and selection variable that minimizes the risk while satisfying the performance constraint that the posterior information matrix for using the selected set of measurements must be larger than the user defined lower bound accuracy J_l.

Allowing for measurement selection and the performance constraint, eqn. (12) becomes:

$$\begin{aligned} P1_a : \min_{x,b} & \left[\|x - x_k^-\|_{P_k^-}^2 + \|\Phi(b)(Hx - z_k)\|_R^2 \right] \\ \text{subject to: } & H^\top R^{-1} \Phi(b) H + J_k^- \geq J_l \\ & b_i \in \{0,1\} \text{ for } i = 1, \ldots, m, . \end{aligned} \tag{14}$$

where $\Phi(b) = diag(b)$. Minor simplifications were made, assuming that R was diagonal and noting that due to the binary definition of b: $b_i^2 = b_i$.

Relaxing the binary constraint on each b_i yields:

$$\begin{aligned} P1_b : \min_{x,b} & \left[\|x - x_k^-\|_{P_k^-}^2 + \|\Phi(b)(Hx - z_k)\|_R^2 \right] \\ \text{subject to: } & H^\top R^{-1} \Phi(b) H + J_k^- \geq J_l \\ & b_i \in [0,1] \text{ for } i = 1, \ldots, m. \end{aligned} \tag{15}$$

which is a convex problem separately in x and b. Based on [17], [27], $P1_b$ can be solved using multi-convex programming by alternatively updating b and x, with the addition of *proximal terms* in the cost function (see below).

The iteration number will be indicated by a right superscript ℓ, starting at zero. To initiate the iterative solution, the two steps of updating b and X are interchangeable. In the ℓ^{th} iteration, $x^{\ell+1}$ and $b^{\ell+1}$ are computed in two steps [17]:

1) *Selecting the measurements:* Optimize the selection vector $b^{\ell+1}$ for fixed x^ℓ by:

$$\begin{aligned} P2 : \min_b & \ \|\Phi(b)(Hx^\ell - z_k)\|_R^2 + \lambda \|b - b^\ell\|^2 \\ \text{subject to: } & J_l - \left(H^\top R^{-1} \Phi(b) H + J_k^- \right) \leq 0 \\ & b_i \in \left[0,1\right] \ \forall i = 1, \cdots, m. \end{aligned}$$

where $\lambda > 0$ is the user-defined proximal parameter. $P2$ is a standard semidefinite programming (SDP) problem and can be solved using an interior point method, and etc.

2) *State update:* Optimize the variable $x^{\ell+1}$ for fixed $b^{\ell+1}$ as:

$$\begin{aligned} P3 : \min_X & \left[\|x - x_k^-\|_{P_k^-}^2 + \|\Phi(b^{\ell+1})(Hx - z_k)\|_R^2 \right. \\ & \left. + \beta \|x - x^\ell\|^2 \right. \end{aligned}$$

where $\beta > 0$ is the user-defined proximal parameter. P3 is an unconstrained least squares optimization problem and can be minimized using QR decomposition, singular value decomposition (SVD), etc.

Remark 1: The method above provides a non-binary selection vector $b_p \in [0,1]^m$. For implementation the designer has at least the following choices.

The designer could specify a threshold τ, such that

$$b_i = \begin{cases} 1 & b_p(i) \geq \tau \\ 0 & otherwise. \end{cases}$$

If $b_i = 0$, the corresponding i^{th} row in H and z_k will be discarded. Using this threshold approach imposes two drawbacks. *a*) The computed accuracy using binary b_i is different than the

solution of the optimization (14) which may not satisfy the lower bound information constraint. *b*) The designer needs to select an appropriate threshold.

Alternatively, the designer could treat $b_p(i) \in [0,1]$ as a measurement information weight to corresponding to the i^{th} row, by replacing H and z_k by $\Phi(b_p)H$ and $\Phi(b_p)z_k$, respectively, in the state estimation process, measurements with smaller $b_p(i)$ are deweighted relative to those with larger values. This is equivalent to replacing the measurement covariance R for that satellite by $\frac{R}{b_p^2(i)}$. △

IV. NUMERICAL RESULTS

This section provides experimental results including comparative studies of performance with Kalman filter, Neyman-Pearson Kalman filter and RAPS algorithms.

A. Hardware and Data Description

The experimental setup included a low-cost single-frequency GPS receiver (u-blox M8T). The antenna was positioned in a previously surveyed location and was stationary. Performance is analyzed using single differenced L1 pseudorange and Doppler. No phase measurements were used. The DGNSS correction data was provided in RTCM standard using NTRIP protocol using a base station ESRI with 14.5 km baseline separation.

B. Algorithm Description

The position estimate algorithm uses a PVA model based Kalman filter approach [28]. The state vector is $x = \left[p^\top,\ v^\top,\ a^\top,\ t_r,\ d_r,\ M_r\right]^\top$. The details of the model are in Section II and of the algorithm are mentioned in Section III. Due to the location of the stationary antenna on the roof of a four story building the sky was clear and there were no obstacles; therefore the collected data set should contained no outliers. This was confirmed by analysis of the KF residuals.

To allow analysis of algorithm performance in the presence of outliers, outliers will be added to the pseudorange measurements in a sequence of Monte Carlo tests. For each Monte Carlo test manually generated outliers are added to two randomly chosen measurements at each time instant. The size of each outlier is drawn from a uniform uniform distribution parameterized by $\mu \in [0.2, 20]$. For $\mu < 4$, the distribution is $U[0,\mu]$. For $\mu >= 4$, the distribution is $U[\mu-4, \mu+4]$. For each Monte Carlo run, the same outlier corrupted data is used for both NPKF and RAPS.

The results are compared with three algorithms:

- **Kalman filter (KF)**: For this algorithm the results include all measurements and no outliers are added. These results show the best possible results in an ideal outlier-free situation.
- **Neyman-Pearson Kalman filter (NP-KF)**: This algorithm has all the measurements available to it, but outliers have been added as described in the previous paragraph. NP-KF applies a threshold test, ignoring all measurements when the absolute value of their residual is greater than the threshold $s_{ii} = \gamma\sqrt{R_{ii} + h_i P_k^- h_i^\top}$ where h_i is the i^{th} row of H and $\gamma = 5$.
- **Risk-Averse Performance-Specified (RAPS)**: This algorithm has all the measurements available to it, but outliers have been added as described in the previous paragraph. RAPS solves the optimization in eqn. (14), which provides a non-binary selection vector $b_p \in [0,1]^m$. Measuremnts are selected by converting b_p to a binary vector as described in Remark 1.

The above mentioned algorithms are used on the same data, with the same outlier corruption, and performance is analyzed.

Peformance analysis includes the norm of position error, sub-meter accuracy percentage, maximum position error. The norm of position error is calculated as:

$$E_{p_k}^n = \|p_r - \hat{p}_k^n\| \tag{16}$$

where p_r is the surveyed antenna position, $\hat{p}_k^n$ is the estimated rover position at time epoch k. The symbol n is the algorithm number. The symbol er_{ps}^n represents the percentage of instances where the position error norm is less that 1 meter.

C. Experimental Results Discussion

Fig. 1 shows the temporal progression of the norm of the position components of the square-root of the diagonal of the computed information matrix for $t \in [588, 595]$ seconds. It is similar for all other time periods. At each integer second a measurement update occurs which increases the information matrix above the black dotted line that shows the lower bound. Between the measurement time instants the position information decreases due to the accumulating propagation uncertainty. The blue curve depicts the information achieved by the KF which uses all measurements at each time step. Note that this is the information that the KF thinks it has, which is true for the outlier free case. If the KF use an outlier-corrupted

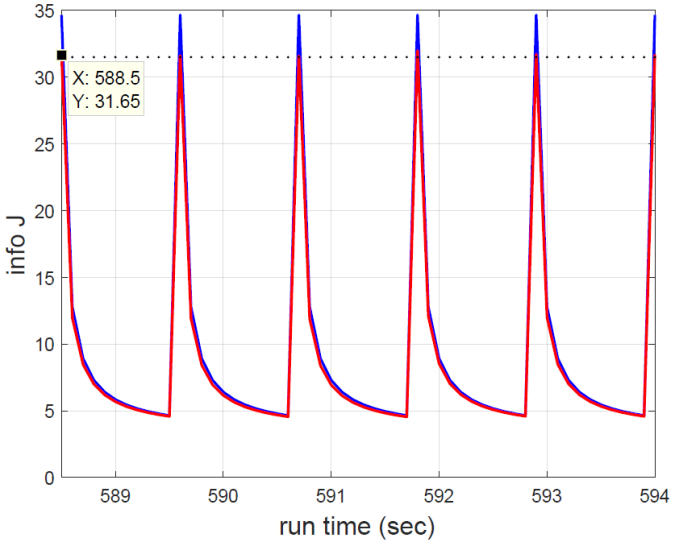

Fig. 1: Position Information Comparison. Blue curve is the Kalman Filter. Red curve is RAPS.

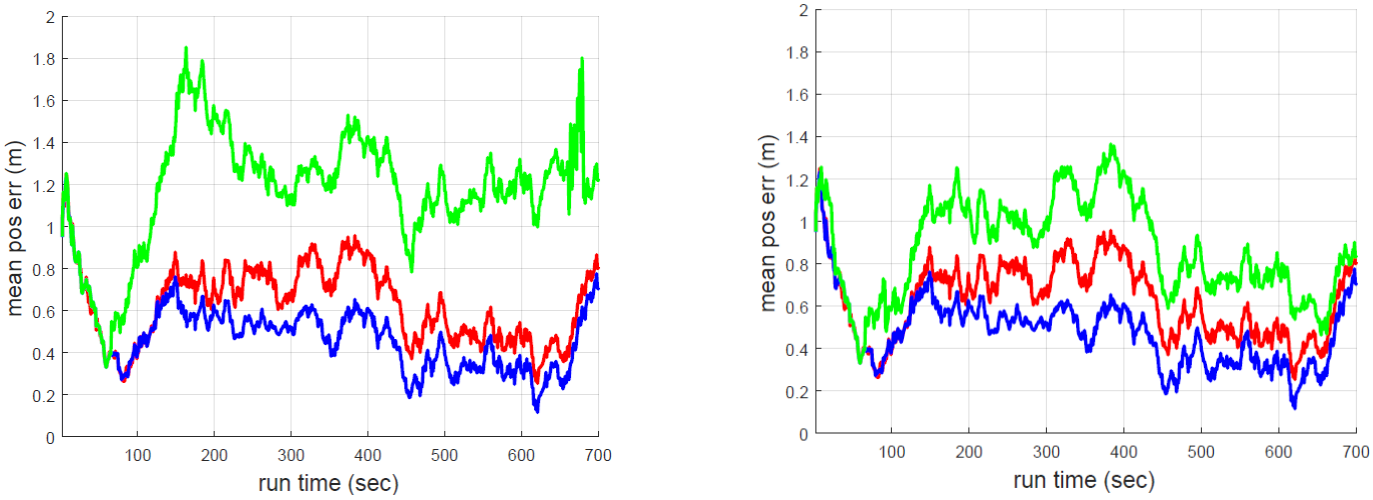

(a) Position Error with $\mu = 8$

(b) Position Error with $\mu = 13$

Fig. 2: Performance Comparison. Red curves are the Kalman Filter. Green curves are for NP-KF. Blue curves are for RAPS.

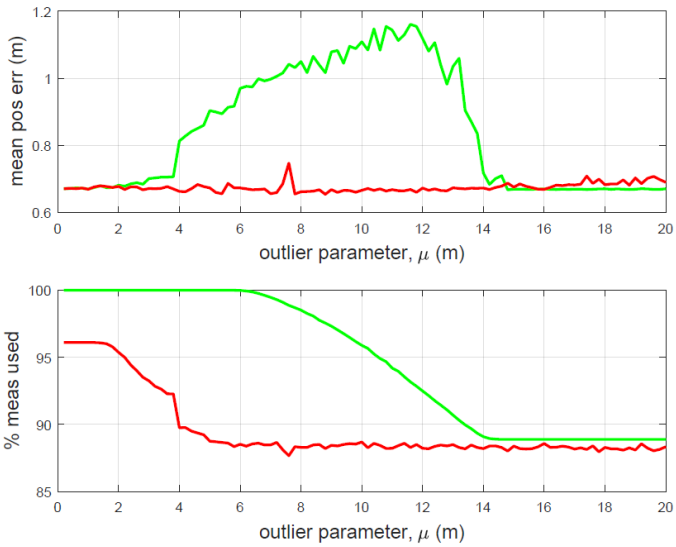

Fig. 3: Position error for outliers of magnitude $[0.2, 20]$. Red curves are RAPS. Green curves are for NP-KF.

TABLE I: Algorithm Comparison (See algorithm description. The KF is outlier free. NP-KF and RAPS have outliers.)

Performance analysis	KF	NP-KF1	NP-KF2	RAPS
Mean of position error (m)	0.55	1.17	0.85	0.59
Std. of position error (m)	0.17	0.28	0.26	0.18
Sub-meter accuracy %	99	19	67	98
Maximum error (m)	1.2	1.8	1.4	1.2

measurement, then the state estimate would be wrong and the information matrix would be too large (over-confident). The red curve shows the progression of the RAPS information matrix. The information increase at the measurement times achieves the lower bound (black curve), but is not as large as the Kalman filter, due to the cost function penalizing risk; therefore, the approach only takes on the amount of risk necessary to achieve the specification.

Figs. 2a and 2b compare the position error for two different scenarios. Each figure shows results from a single 1000 second experiment. The blue curve is the KF without outliers, representing the best performance achievable for the given dataset, without outliers. The red and green curves represent the performance of RAPS and NP-KF when outliers are added. In Fig. 2a the outlier parameter $\mu = 8$. In Fig 2b the outlier parameter $\mu = 13$. In both figures, the RAPS performance is not quite as good as the KF (no outliers), but better than NP-KF. The performance of the NP-KF is better in Fig 2b ($\mu = 13$) than it is in Fig. 2a ($\mu = 13$), because the larger magnitude of the outlier results in the threshold test being more successful in detecting and removing outliers correctly.

It is important to note that the RAPS approach does not simply use the smallest residuals. Selecting the smallest residuals might not satisfy the performance constraint, because the corresponding rows of the H matrix may not be sufficiently diverse. In the RAPS approach, the optimization process ensures that the selected measurements result in sufficient diversity in the rows of H to satisfy the position error specification, while minimizing the risk of including outliers. As the number of measurements increases, the expected information from those measurement increases, but so does the risk of inclusion of outliers. The RAPS may ignore some of the smaller residuals, as they would add risk without supplying a sufficient amount of new information. In the RAPS approach the number of measurements used at each time may vary. In this experiment, over 60% of the measurements at each time are used.

Table I summarizes various measures of positioning accuracy for $[0, 1000]$ seconds of data with two different scenarios: *a*) The outlier magnitude is $\mu = 8$. The results are presented in the column headed by *NP-KF1*. *b*) The outlier magnitude is $\mu = 13$. The results are presented in the column headed by *NP-*

KF2. The RAPS results for the two scenarios were the same to within centimeters of accuracy. The first and second rows compare the mean and standard deviation (std) of position error defined in eqn. (16). Rows 3 reports the percentage of samples that achieved sub-meter accuracy. That paper using KF methods shows 99% of samples achieving submeter accuracy over 1000 seconds of data while using RAPS yields to 98% of submeter accuracy. The RAPS approach performs better that the NP-KF approach in both scenarios by all measures.

Fig. 3 shows the NP-KF and RAPS performance, averaged over 20 Monte Carlo simulations. To produce one point on the curve for one value of $\mu \in [0.2, 20]$ meter: twenty experiment were each run over $[0, 1000]$ seconds; the position error at each second were computed; the position errors were averaged both over the 1000 seconds and the 20 Monte Carlo experiments. Each Monte Carlo experiment generate a new set of outliers that was used both for NP-KF and RAPS. With nine satellites available and two outliers per epoch, the measurement set (pseudorange plus Doppler) contains 11% outliers. The red curves displays the result for the RAPS algorithm. The green curves displays the results for NP-KF approach. The y-axis in the top figure is the mean of the error. The y-axis in bottom figure is the percentage of the measurements are used for state estimation. NP-KF uses all measurements when μ is small. Then its threshold test removes an increasingly higher percentage of the outliers correctly as the magnitude of the outlier increases, until it is correctly removing 11% of the pseudoranges. Therefore, NP-KF mean error initially rises and later falls as the magnitude of the outlier increases. RAPS mean position error performance is robust to the magnitude of the outlier.

V. CONCLUSIONS

Many applications require reliable, high precision state estimation consistent with (i.e., sub-meter) position accuracy. Success requires mitigation of measurement outliers. This paper applied the risk-averse performance-specified (RAPS) method [17] to estimate the rover state using GNSS measurements. In this paper, the feasibility of the proposed approach has been demonstrated and performance was evaluated relative to a Neyman-Pearson Kalman Filter with the same outlier sets and to an outlier free Kalman filter using experimental data. Performance is summarized in Figs. 2a and 2b and Table I. RAPS successfully estimated the rover state with horizontal position accuracy at the submeter level for 98% of the samples. The mean and standard deviation of the position error using RAPS are 59 cm and 18 cm, respectively. The comparisons herein are limited. Further comparison as a function of the NP-KF threshold γ and the number of measurements affected by outliers are also of interest. A companion paper at this conference [29] discusses and compares KF algorithms and a differential correction computation approach to maintain accuracy in the presence of communication latency.

The proposed approach is not limited to GNSS state estimation, but can be beneficially applied to other domains where outliers have to be suspected, such as SLAM , machine learning, etc. Implementation in other applications and comparison with alternative methods proposed by other authors are of interest for future work. Moreover, in this article an interior point method is employed to solve the SDP optimization problem (14) which is time-consuming and the computational cost grows as the number of measurements increases. Future research can focus on enhancing computational efficiency toward real-time solution, application to moving data sets, and application with inertial sensors.

ACKNOWLEDGMENT

This work was partially supported by NSF grant IIS-1316934 and Sirius XM. We gratefully acknowledge these supports. All opinions expressed in this article are those of the authors.

REFERENCES

[1] P. Teunissen and O. Montenbruck, *Springer handbook of global navigation satellite systems*. Springer, 2017.
[2] J. Neyman and E. S. Pearson, "The testing of statistical hypotheses in relation to probabilities a priori," in *Mathematical Proceedings of the Cambridge Philosophical Society*, vol. 29, no. 4. Cambridge University Press, 1933, pp. 492–510.
[3] A. S. Willsky, "A survey of design methods for failure detection in dynamic systems," *Automatica*, pp. 601–611, 1976.
[4] E. Y. Chow and A. S. Willsky, "Issues in the development of a general design algorithm for reliable failure detection," 1980.
[5] E. Chow and A. Willsky, "Analytical redundancy and the design of robust failure detection systems," *IEEE Transactions on automatic control*, vol. 29, no. 7, pp. 603–614, 1984.
[6] R. A. Fisher, "Statistical methods for research workers," in *Breakthroughs in Statistics*. Springer, 1992, pp. 66–70.
[7] R. J. Patton and J. Chen, "Review of parity space approaches to fault diagnosis for aerospace systems," *Journal of guidance control and dynamics*, vol. 17, pp. 278–278, 1994.
[8] R. G. Brown, "A baseline GNSS RAIM scheme and a note on the equivalence of three RAIM methods," *Navigation*, vol. 39, no. 3, pp. 301–316, 1992.
[9] ——, "Solution of the Two-Failure GPS RAIM Problem Under Worst-Case Bias Conditions: Parity Space Approach," *Navigation*, pp. 425–431, 1997.
[10] R. Brown and P. Hwang, "From RAIM to NIORAIM A New Integrity Approach to Integrated Multi-GNSS Systems," *Inside GNSS, May-June*, 2008.
[11] M. A. Sturza, "Navigation system integrity monitoring using redundant measurements," *Navigation*, vol. 35, no. 4, pp. 483–501, 1988.
[12] R. Patton, "Fault detection and diagnosis in aerospace systems using analytical redundancy," *Computing & Control Engineering Journal*, pp. 127–136, 1991.
[13] J. Angus, "RAIM with multiple faults," *Navigation*, pp. 249–257, 2006.
[14] S. Weisberg, *Applied linear regression*. John Wiley & Sons, 2005, vol. 528.
[15] S. Hewitson and J. Wang, "Extended receiver autonomous integrity monitoring (E RAIM) for gnss/ins integration," *Journal of Surveying Engineering*, vol. 136, pp. 13–22, 2010.
[16] L. Carlone, A. Censi, and F. Dellaert, "Selecting good measurements via l1 relaxation: A convex approach for robust estimation over graphs," in *IROS*. IEEE, 2014, pp. 2667–2674.
[17] E. Aghapour and J. A. Farrell, "Performance specified state estimation with minimum risk," *American Control Conference*, 2018.
[18] J. Wright, A. Y. Yang, A. Ganesh, S. S. Sastry, and Y. Ma, "Robust face recognition via sparse representation," *IEEE transactions on pattern analysis and machine intelligence*, vol. 31, no. 2, pp. 210–227, 2009.
[19] X. Mei and H. Ling, "Robust visual tracking using l1 minimization," in *Computer Vision*. IEEE, 2009, pp. 1436–1443.
[20] D. Wang, H. Lu, and M.-H. Yang, "Robust visual tracking via least soft-threshold squares," *IEEE Transactions on Circuits and Systems for Video Technology*, vol. 26, pp. 1709–1721, 2016.

[21] P. Huber, *Robust Statistics*. New York, John Wiley and Sons Inc, 1981.
[22] A. M. Leroy and P. J. Rousseeuw, "Robust regression and outlier detection," *New York: Wiley, 1987*, 1987.
[23] S. Zhao, Y. Chen, H. Zhang, and J. A. Farrell, "Differential GPS aided inertial navigation: A contemplative realtime approach," *IFAC*, pp. 8959–8964, 2014.
[24] P. F. Roysdon and J. A. Farrell, "Robust GPS-INS Outlier Accommodation: A Soft-thresholded Optimal Estimator," *IFAC*, pp. 3574–3579, 2017.
[25] J. Farrell, *Aided navigation: GPS with high rate sensors*. McGraw-Hill, Inc., 2008.
[26] S. Thrun, W. Burgard, and D. Fox, *Probabilistic robotics*. MIT press, 2005.
[27] X. Shen, S. Diamond, M. Udell, Y. Gu, and S. Boyd, "Disciplined multi-convex programming," in *Control And Decision Conference*. IEEE, 2017, pp. 895–900.
[28] R. Brown and P. Hwang, *"Introduction to Random Signals and Applied Kalman Filtering"*. Wiley, New York, 1996.
[29] F. Rahman, E. Aghapour, and J. A. Farrell, "ECEF Position Accuracy and Reliability in the Presence of Differential Correction Latency ," *Proc. of IEEE/ION PLANS, in press*, 2018.